Journal of Materials Chemistry C

PAPER

View Article Online
View Journal | View Issue

Cite this: J. Mater. Chem. C, 2019, 7, 14678

Donor–acceptor copolymers with 1,7-regioisomers of *N,N′*-dialkylperylene-3,4,9,10-tetracarboxydiimide as materials for photonics†

Věra Cimrová,* Drahomír Výprachtický, Veronika Pokorná and Petra Babičová

Received 23rd September 2019,
Accepted 4th November 2019

DOI: 10.1039/c9tc05233j

rsc.li/materials-c

Donor–acceptor (D–A) copolymers containing *N,N′*-dialkylperylene-3,4,9,10-tetracarboxydiimide electron-acceptor units with dodecyl (**DDPDI**) or 2-ethylhexyl (**EHPDI**) substituents and three different electron-donor units (9,9-dioctylfluorene, 9-(2-ethylhexyl)carbazole or 9-(heptadecan-9-yl)carbazole) were synthesized by Suzuki coupling and were then characterized. Their thermal, photophysical, electrochemical and spectroelectrochemical properties were studied. The effects of the alkyl side chain combination on the properties were evaluated and are discussed. Despite large differences in the absorption spectra of the individual **DDPDI** and **EHPDI** units or monomers in solutions and thin films, the absorption spectra of the copolymers in solutions and thin films exhibited similar shapes. More pronounced side chain effects were observed in the photoluminescent (PL) behaviour than in the absorption behaviour. Different alkyl side chains on the D–A copolymers similarly affected the visible absorption band contributions in the solutions and thin films, but the exhibited effects were different for the PL spectra and efficiency. The copolymers exhibited reversible reduction and irreversible oxidation. The ionization potential and bandgap values were influenced by the donor unit and by the perylene-3,4,9,10-tetracarboxydiimide (PDI) side chain nature. Spectroelectrochemical changes are reported, and potential sensing applications are outlined.

Introduction

Perylene-3,4,9,10-tetracarboxydiimide derivatives, also commonly called perylene diimides (PDIs), have been extensively studied as industrial colorants, both as dyes (soluble) and pigments (insoluble) for many years. To date, PDIs have been utilized in various electronic and optical applications, such as organic field-effect transistors and phototransistors,[1–6] fluorescent solar collector or luminescent solar concentrators,[7–10] electrophotographic devices,[11] dye lasers,[12] organic photovoltaic cells,[13–19] sensing[20–25] and optical power limiters,[26] and in batteries[27–30] due to their specific physical, optical, and/or electronic properties.

PDIs represent an interesting class of n-type semiconductors in the field of organic electronics.[31,32] PDI was used as a building block for organic solar cells (OSCs) with bulk heterojunctions (BHJ) based on non-fullerene small molecule acceptors due to its good chemical, thermal, and light stabilities, strong electron-withdrawing ability, and high electron mobility.[14,33,34] However, monomeric PDI possesses a highly planar conformation and thus strong intermolecular π–π stacking,[22] which leads to large crystalline domain formation and severe donor–acceptor phase separation in BHJ films. The self-trapping of excitons in the domains of strongly aggregated PDI molecules is the main reason for the low efficiency of perylene-based devices.[34] Therefore, one of the most important design principles for the development of efficient PDI-based non-fullerene small molecule acceptors for use in OSCs is the restriction of self-aggregation among planar PDI.[35] Therefore, focus has also been on the synthesis of PDI-based polymers, which were reported as potential n-type materials for all-polymeric solar cells.[17,36–39] Furthermore, PDIs are also interesting as interfacial materials (electron transporting layers) to reduce interface trap density not only in organic solar cells but also in perovskite solar cells.[40,41] Doped PDIs have been demonstrated to have tremendously enhanced electrical properties.[23,42–45] For the application of PDI-based polymers, it is also important to understand how their optical and electrochemical properties can be tuned by various donors or *via* attachment of different side chains on the perylene core or to the donor units. For the purposes mentioned above, the optical and electronic properties are of interest in relation to the polymeric chemical structure such as the composition of the main backbone as well as the sidechain nature and their combination. Therefore, we focus on the synthesis of a series of donor–acceptor copolymers with PDI acceptor units with various combinations of side chains and a comprehensive study of their photophysical and

Institute of Macromolecular Chemistry, Czech Academy of Sciences, Heyrovsky Sq. 2, 16206 Prague 6, Czech Republic. E-mail: cimrova@imc.cas.cz

† Electronic supplementary information (ESI) available. See DOI: 10.1039/c9tc05233j

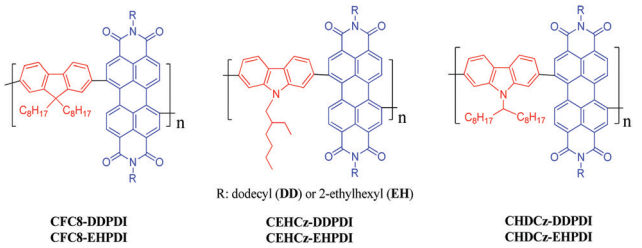

Fig. 1 Chemical structure of the copolymer series poly[*N*,*N*′-dialkylperylene-3,4,9,10-tetracarboxydiimide-1,7-diyl-*alt*-9-alkylcarbazole-2,7-diyl or 9,9-dioctylfluorene-2,7-diyl]s.

electronic properties. To the best of our knowledge, there are no detailed photophysical and spectroelectrochemical studies performed on such PDI-based polymers.

In this work, we report on a series of six donor–acceptor (D–A) copolymers containing *N*,*N*′-dialkylperylene-3,4,9,10-tetracarboxydiimide electron-acceptor (A) units (strictly as 1,7-regioisomers) and three different electron donor (D) units [9,9-dioctylfluorene, 9-(2-ethylhexyl)carbazole or 9-(heptadecan-9-yl)carbazole], namely, poly[*N*,*N*′-dialkylperylene-3,4,9,10-tetracarboxydiimide-1,7-diyl-*alt*-9-alkylcarbazole-2,7-diyl or 9,9-dioctylfluorene-2,7-diyl]s (Fig. 1). The copolymers were successfully synthesized by Suzuki coupling and were then characterized. The necessary acceptor monomers *N*,*N*′-bis(2-ethylhexyl)-1,7-dibromoperylene-3,4,9,10-tetracarboxydiimide (**EHPDI-Br**) and *N*,*N*′-didodecyl-1,7-dibromoperylene-3,4,9,10-tetracarboxydiimide (**DDPDI-Br**) were synthesized, and the purification of 1,7-isomers was described. The thermal stability, photophysical and electrochemical properties of the copolymers were investigated and discussed with the aim of obtaining information about the influence of the PDI substitution and side chain configuration on the photophysical and electrochemical properties of the copolymers. The effects of alkyl chains (dodecyl or 2-ethylhexyl) attached to the nitrogen of the PDI unit on properties of the copolymers were studied and are shown. Furthermore, a spectroelectrochemical study on the copolymers was performed with the aim of obtaining information about the electrochromic properties with respect to potential sensing applications. Electrochromic changes during oxidation and reduction are reported and discussed.

Results and discussion

Synthesis of acceptor-monomers EHPDI-Br and DDPDI-Br

Scheme 1 shows perylene-3,4,9,10-tetracarboxylic dianhydride (**I**), which can be considered the precursor compound of this class of substances. PDIs with different chemical and physical properties have been obtained by modification of the substituents, most often those in the imide *N*,*N*′ positions and the 1, 6, 7, and 12 positions (so-called "bay" positions). The condensation reaction between **I** and an alkyl amine or an aniline results in the formation of the appropriate PDI derivative, usually in high yield.[46] Dibromo derivatives of PDIs are key intermediates for the synthesis of a wide range of other bay-substituted derivatives and are generally obtained by imidization of the corresponding halogenated **I** derivatives. In a 1997 BASF patent,[47] conditions (Br_2, 100% H_2SO_4, I_2 as a catalyst, 85 °C) were developed for the bromination of **I**. This patent claimed that the bromination of perylene dianhydride **I** under the applied conditions selectively forms 1,7-dibromoperylene dianhydride, and consequently, the subsequent imidization leads to isomerically pure 1,7-dibrominated PDI. F. Würthner *et al.* reported[48] that the functionalized PDIs were apparently mixtures of 1,7-, 1,6-, and 1,6,7-regioisomers rather than isomerically pure compounds, which can be observed by high-field (>400 MHz) ^{1}H NMR only. They proved that bromination of **I** after the patented procedure[47] gave a mixture of 1,7-, 1,6-, and 1,6,7-brominated perylene dianhydrides, which are insoluble in organic solvents and, therefore, could not be purified by any means. The crude product was used for the subsequent imidization with cyclohexylamine, and the expected mixture of soluble 1,7-, 1,6-, and 1,6,7-brominated PDIs was separated by column chromatography (CH_2Cl_2) and repetitive crystallization (CH_2Cl_2/MeOH = 1 : 1 v/v). Later, B. Rybtchinski *et al.* reported[49] that bromination and imidization (2,4-dimethylpentan-3-amine) can be interchanged; in other words, the bromination of the prepared PDIs led to a similar mixture of brominated PDI regioisomers, which could be separated by column chromatography (CH_2Cl_2) and repetitive crystallization (CH_2Cl_2/hexane = 1 : 1 v/v). Taking into account both reports[48,49] and the reviewed syntheses of PDI derivatives,[50] we prepared the acceptor monomers **EHPDI-Br**

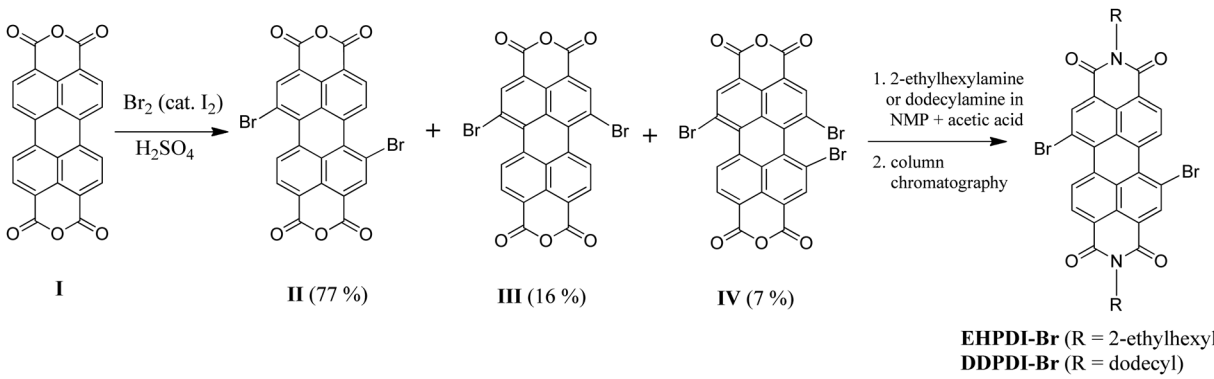

Scheme 1 Synthesis of *N*,*N*′-bis(2-ethylhexyl)-1,7-dibromoperylene-3,4,9,10-tetracarboxy-diimide (**EHPDI-Br**) and *N*,*N*′-didodecyl-1,7-dibromoperylene-3,4,9,10-tetracarboxydiimide (**DDPDI-Br**) from perylene-3,4,9,10-tetracarboxylic dianhydride (**I**).

and **DDPDI-Br** as follows (Scheme 1). The bromination of perylene-3,4,9,10-tetracarboxylic dianhydride (**I**) was performed in 100% sulfuric acid at 85 °C using iodine as a catalyst according to a published procedure.[47,48] The crude product, which is insoluble in organic solvents, was explored by 600 MHz ^{1}H NMR in deuterated sulfuric acid-d_2 (96–98 wt% in D_2O). Three sets of signals with different intensities were observed in the ^{1}H NMR spectrum (Fig. S1, ESI†), indicating that at least three different products were formed in the bromination of dianhydride **I**. In the region 8.46–8.62 ppm, three doublets appeared, then at 8.67, 8.69 and 8.72 ppm, three singlets appeared, and finally, three doublets overlapped to form a multiplet at 9.26–9.45 ppm. This signal pattern implies that a mixture of 1,7- (**II**), 1,6- (**III**), and 1,6,7-brominated perylene (**IV**) dianhydrides was prepared as expected.[48] The integration areas of the singlets at 8.72 (**II**), 8.69 (**III**), and 8.67 (**IV**) ppm revealed that the products were formed in a **II**:**III**:**IV** ratio of *ca.* 77:16:7 (wt%). The results of elemental analysis of the mixture were in good agreement with the NMR data. To eliminate the formation of tribromo derivative **IV**, we tried a low-temperature bromination procedure (a published[51] temperature of 40 °C), but in this case, the bromine content in crude material was too low (7.26% *vs.* 29.05% calcd for **II**). Since the brominated perylene dianhydrides **II**, **III**, and **IV** are insoluble in organic solvents, the crude product mixture was used for subsequent imidization with 2-ethyl-1-hexylamine or *n*-dodecylamine to obtain *N*,*N*′-bis(2-ethylhexyl)-1,7-dibromoperylene-3,4,9,10-tetracarboxydiimide (**EHPDI-Br**) or *N*,*N*′-didodecyl-1,7-dibromoperylene-3,4,9,10-tetracarboxydiimide (**DDPDI-Br**), respectively (Scheme 1). The syntheses took place smoothly in *N*-methyl-2-pyrrolidone/glacial acetic acid at 120 °C under argon. **EHPDI-Br** was purified by column chromatography on silica gel using dichloromethane/hexane (4:1 v/v) as the eluent. The fractions with the 1,7-dibromo derivative **EHPDI-Br** (R_F = 0.47, TLC in the same solvent) were separated from the 1,6,7-tribromo derivative (R_F = 0.70) and 1,6-dibromo derivative (R_F = 0.32). The purity of **EHPDI-Br** was confirmed by 600 MHz ^{1}H NMR (Fig. S2, ESI†), where the 1,7-doublets at 9.405 (J = 7.8 Hz) and 8.626 (J = 7.8 Hz) ppm were clear without any notable presence of 1,6-doublets (*cf.* ref. 48 and 49). **DDPDI-Br** was purified by column chromatography on silica gel using dichloromethane as the eluent. The fractions with the 1,7-dibromo derivative **DDPDI-Br** (R_F = 0.41, TLC in CH_2Cl_2/hexane = 3:1 v/v) were separated from the 1,6,7-tribromo derivative (R_F = 0.56) and 1,6-dibromo derivative (R_F = 0.20). The purity of **DDPDI-Br** was confirmed by 600 MHz ^{1}H NMR (Fig. S3, ESI†), where the 1,7-doublets at 9.378 (J = 8.4 Hz) and 8.597 (J = 7.8 Hz) ppm were clear without any notable presence of 1,6-doublets. The ^{13}C NMR (150.96 MHz) spectra support the proposed structures of **EHPDI-Br** (Fig. S4, ESI†) and **DDPDI-Br** (Fig. S5, ESI†). Unlike ref. 48 and 49 we did not need to apply repetitive crystallization following column chromatography to obtain pure 1,7-derivatives. The chromatographic selectivity of the *N*-alkyl substituents used (2-ethyl-1-hexyl-, *n*-dodecyl-) probably brings about better chromatographic separation of the 1,6-di-, 1,7-di-, and 1,6,7-tribrominated regioisomers for synthesis of the pure acceptor-monomers **EHPDI-Br** and **DDPDI-Br** than the reported cyclohexyl-[48] or 2,4-dimethyl-3-pentyl-[49] substituents.

Synthesis of D–A copolymers

The poly[*N*,*N*′-dialkylperylene-3,4,9,10-tetracarboxydiimide-1,7-diyl-*alt*-9-alkylcarb-azole-2,7-diyl or 9,9-dioctylfluorene-2,7-diyl]s (D–A copolymers) were synthesized by Suzuki coupling (THF/aq. 2 M Na_2CO_3, $Pd(PPh_3)_4$ as a catalyst, 85 °C, 66 h) of the corresponding donor (**FC8-B**, **EHCz-B**, or **HDCz-B**) and acceptor (**EHPDI-Br** or **DDPDI-Br**) comonomers. The polymerization proceeded smoothly, and the syntheses, structure, and abbreviations of the prepared copolymers are shown in Scheme 2. The synthesized D–A copolymers were characterized by size-exclusion chromatography (SEC, M_w, M_n, $Đ = M_w/M_n$, P) in chloroform (Table 1 and Fig. 2) and by ^{1}H, ^{13}C NMR (Fig. S6–S17, ESI†) and FTIR (Fig. S18–S23, ESI†) spectroscopy. The copolymers with **DDPDI** (linear dodecyl side chains on PDI) possessed higher M_w values than the corresponding copolymers with **EHPDI** (branched side chains on PDI) units. The FTIR spectra were similar to each other and exhibited

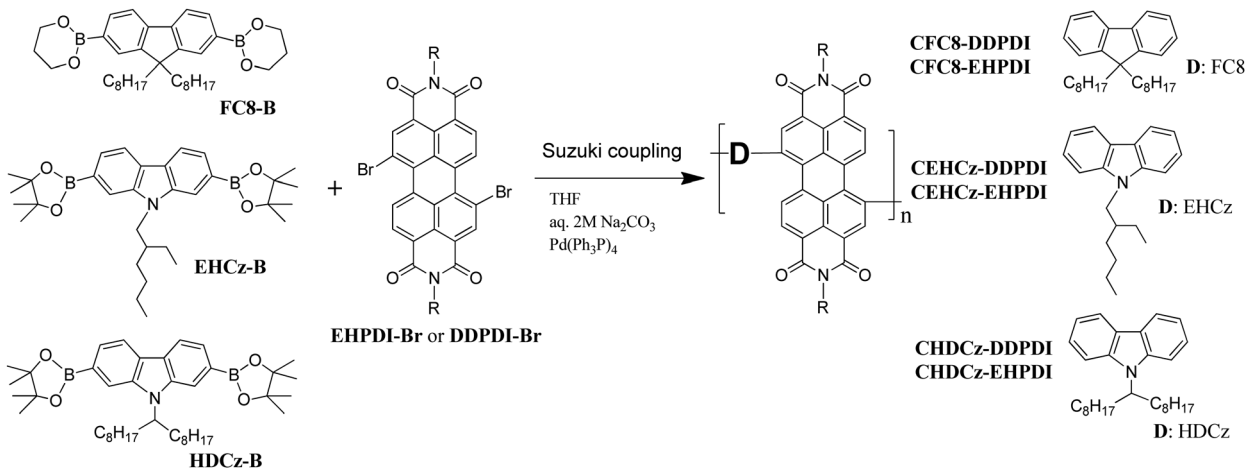

Scheme 2 Synthesis of D–A copolymers under study, *i.e.*, the poly[*N*,*N*′-dialkylperylene-3,4,9,10-tetracarboxydiimide-1,7-diyl-*alt*-9-alkylcarbazole-2,7-diyl or 9,9-dioctylfluorene-2,7-diyl]s, by Suzuki coupling.

Table 1 Size-exclusion chromatography (SEC) data[a] for the D–A copolymers (M_w is the weight-average molecular weight, M_n is the number-average molecular weight, $Đ$ is the dispersity, and P is the polymerization degree)

Copolymer	D	R	M_w	M_n	$Đ$	P
CFC8-DDPDI	FC8	DD (dodecyl)	27 000	17 000	1.59	24
CFC8-EHPDI	FC8	EH (2-ethylhexyl)	13 230	9500	1.39	13
CEHCz-DDPDI	EHCz	DD (dodecyl)	37 700	19 920	1.89	37
CEHCz-EHPDI	EHCz	EH (2-ethylhexyl)	28 570	14 030	2.04	32
CHDCz-DDPDI	HDCz	DD (dodecyl)	34 568	25 185	1.37	30
CHDCz-EHPDI	HDCz	EH (2-ethylhexyl)	27 640	19 900	1.39	27

[a] Measured by SEC in chloroform as the mobile phase; polystyrene standards were used for calibration.

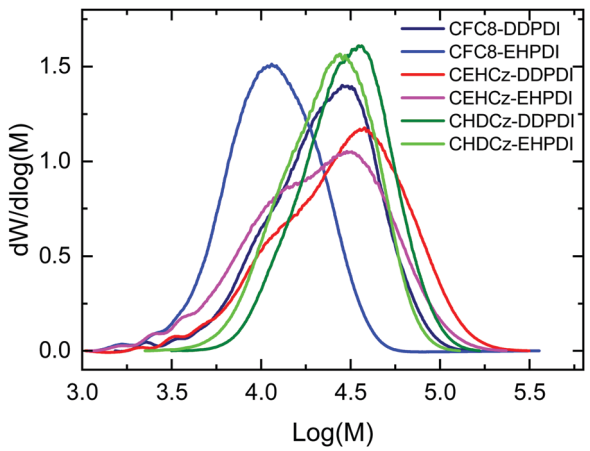

Fig. 2 SEC curves of the D–A copolymers under study measured in chloroform as the mobile phase. Polystyrene standards were used for calibration.

vibration bands at 2959–2918 cm^{-1} (assigned to aromatic CH stretching), 2860–2850 cm^{-1} (assigned to aliphatic CH stretching), 1701–1698 cm^{-1} (assigned to symmetric C=O stretching), 1661–1653 cm^{-1} (assigned to antisymmetric C=O stretching), 1588–1581 cm^{-1} (assigned to aromatic ring stretching), 1460–1400 cm^{-1} (assigned to the aliphatic CH_2 scissoring vibration and CH_3 deformation), 1326–1322 cm^{-1} (assigned to C–N stretching), 1245–1242 cm^{-1} (assigned to C–N–C stretching), 1180–1000 cm^{-1} (assigned to the C–C stretching in alkyls), 860–808 cm^{-1} (assigned to the CH out-of-plane deformation), 760–710 cm^{-1} (assigned to CH_2 rocking in alkyls), and 640–625 cm^{-1} (assigned to in-plane ring deformation). In the ^1H NMR spectrum, the peaks of the aromatic protons were found at 9.10–7.25 ppm, and the peaks of the aliphatic protons were found at 4.60–4.55 ppm (Cz-N–CH=), 4.13–4.19 ppm (Per-N–CH_2), and 2.60–0.50 ppm with sufficiently distinguished broad peaks of the fluorene–CH_2, =CH–, Per-N–C–CH_2, Cz-N–C–CH_2, CH_2 and CH_3 protons. The ratio of the aliphatic to aromatic integrals confirmed the structure of the repeating polymer unit –[D–PDI]$_n$–, as shown in Scheme 2. In the ^{13}C NMR spectrum, the peaks of the C=O (167.7–163.5 ppm), aromatic (156.2–108.8 ppm) and aliphatic (58.8–10.7 ppm) carbons were separated. The signals of =C(octyl)$_2$ (58.8, 56.3 ppm), Cz-N–C (50.3, 47.6 ppm), and Cz-N–C< (56.6, 56.9 ppm) were assigned. Unlike in our recently published

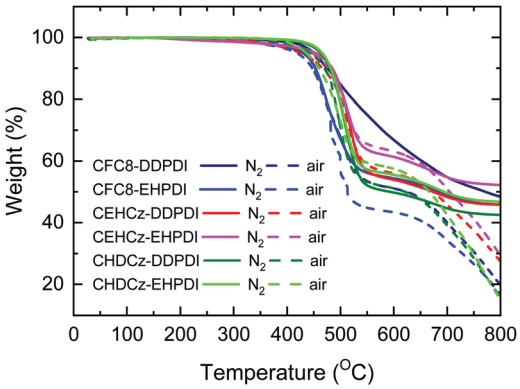

Fig. 3 TGA curves of copolymers measured at a scan rate of 10 K min^{-1} in N_2 (solid) and in air (dashed).

Table 2 The thermal properties of the D–A copolymers ($T_{d5\%}$ and $T_{d10\%}$ are the decomposition temperatures at which 5% and 10% weight losses were recorded, respectively, and W_{res} is the residual weight percentage at 800 °C under N_2)

	$T_{d5\%}$ (°C)		$T_{d10\%}$ (°C)		W_{res} (%)
Polymer	N_2	Air	N_2	Air	N_2
CFC8-DDPDI	450	433	475	452	48
CFC8-EHPDI	429	417	453	447	46
CEHCz-DDPDI	449	425	484	467	46
CEHCz-EHPDI	453	444	484	478	56
CHDCz-DDPDI	462	442	480	470	43
CHDCz-EHPDI	466	436	482	460	47

paper,[52] we were not successful here with short-time Suzuki coupling in a high-boiling point solvent. Using a xylene/aq. saturated $NaHCO_3$ system (130 °C, 30 min) and $Pd(PPh_3)_4$ as a catalyst, only the low-molecular-weight products (M_w = 1500, M_n = 1100) were obtained.

Thermal properties

The thermal stability of the synthesized copolymers was investigated by thermogravimetric analysis (TGA). The TGA curves measured in N_2 and in air at a heating rate of 10 K min^{-1} are shown in Fig. 3. The temperatures for 5% and 10% weight losses and the residual weight percentages are given in Table 2. The copolymers exhibited very good thermal stability in nitrogen and in air, as reflected by the weight loss results. The residual weight percentage at 800 °C in N_2 reflects the high aromatic content, and weight loss was caused by decomposition of the alkyl side chains. Very good thermal stability in air also indicates good oxidation stability.

Photophysical properties

The photophysical properties of the new copolymers and the PDI units and monomers were studied in chloroform and 1,2-dichlorobenzene (DCB) solutions and in thin films. The absorption spectra of the chloroform solutions are displayed in Fig. 4, where the spectra of **DDPDI**, **EHPDI** and **DDPDI-Br**, **EHPDI-Br** are shown for comparison. The absorption maxima are summarized in Table 3. The solution absorption spectra of

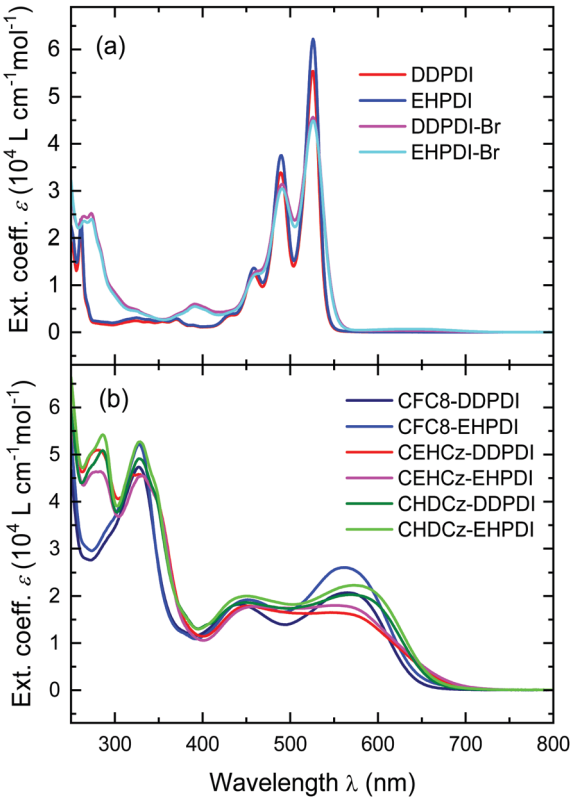

Fig. 4 UV-vis absorption spectra of (a) the **DDPDI** and **EHPDI** units and the **DDPDI-Br** and **EHPDI-Br** monomers, and (b) the copolymers under study measured in dilute chloroform solutions.

Table 3 Photophysical properties of the copolymers measured in dilute chloroform solutions (λ_{absmax}: absorption maximum; λ_{PLmax}: emission maximum; η_{PL}: photoluminescence quantum yield). The main maxima in the visible region are printed in bold

Copolymer	λ_{absmax} (nm)	λ_{PLmax}[a] (nm)	η_{PL}
DDPDI	261, 433, 458, 489, **526**	**534**, 576, 620	0.978
EHPDI	261, 431, 459, 490, **526**	**535**, 575, 621	0.957
DDPDI-Br	272, 391, 460 sh, 491, **526**	**546**, 581	0.865
EHPDI-Br	272, 391, 460 sh, 491, **526**	**547**, 582	0.844
CFC8-DDPDI	327, 442, **565**	**661**	0.205
CFC8-EHPDI	328, 451, **563**	**660**	0.149
CEHCz-DDPDI	279, 327, **451**, 546	**698**	0.016
CEHCz-EHPDI	283, 331, 461, **553**	**696**	0.021
CHDCz-DDPDI	286, 328, 450, **570**	**680**	0.043
CHDCz-EHPDI	286, 329, 451, **573**	**679**	0.049

[a] Excitation wavelength at 483 nm.

DDPDI and **EHPDI** exhibited a clear vibration structure with a main maximum at 526 nm. In **DDPDI-Br** and **EHPDI-Br**, the Br substitution in bay positions led to the broadening of the absorption bands in the solution spectra as a result of the Franck–Condon progression in vibration modes. The main maximum remained at the same position of 526 nm, and an additional broad UV absorption peak from 270 nm to 330 nm and a new band with a maximum at 391 nm appeared.

The absorption spectra of the copolymers consisted of broad bands in the visible spectral region corresponding to π–π* transition of the conjugated backbone. The copolymers **CFC8-DDPDI** and **CFC8-EHPDI** with fluorene D units showed maxima at 328 nm in the UV spectral region and broad band absorption from 400 nm to 650 nm in the visible spectral region with two well-resolved maxima at 440–450 and 560–565 nm. In the absorption spectra of the copolymers with carbazole D units, an additional peak at 279–286 nm was observed, which is typical for the absorption of the carbazole D unit. The absorption spectra in the visible region of the copolymers **CEHCz-DDPDI** and **CEHCz-EHPDI** with carbazole D units were less resolved than those of copolymers with fluorene D units or **CHDCz-DDPDI** and **CHDCz-EHPDI** with carbazole D units with long branched chains. This fact reflects differences in backbone conformations.

The absorption spectra of thin films are displayed in Fig. 5. The absorption spectra of **DDPDI**, **EHPDI** and **DDPDI-Br**, **EHPDI-Br** thin films differed significantly when compared with their spectra in solutions due to molecular aggregation.[53,54] The absorption spectra of the copolymer thin films differed only slightly from the absorption spectra of their solutions in terms of the mutual contributions of bands in the visible regions to the overall absorption. In the solutions, the contribution of the longest wavelength band was higher than that in thin films. This could be explained by the different backbone conformations in the solutions and in thin films. In thin films, improved backbone planarity is expected. The contribution of these visible bands to UV bands in thin films is also slightly influenced by the thickness. The absorption maxima are summarized in Table 4.

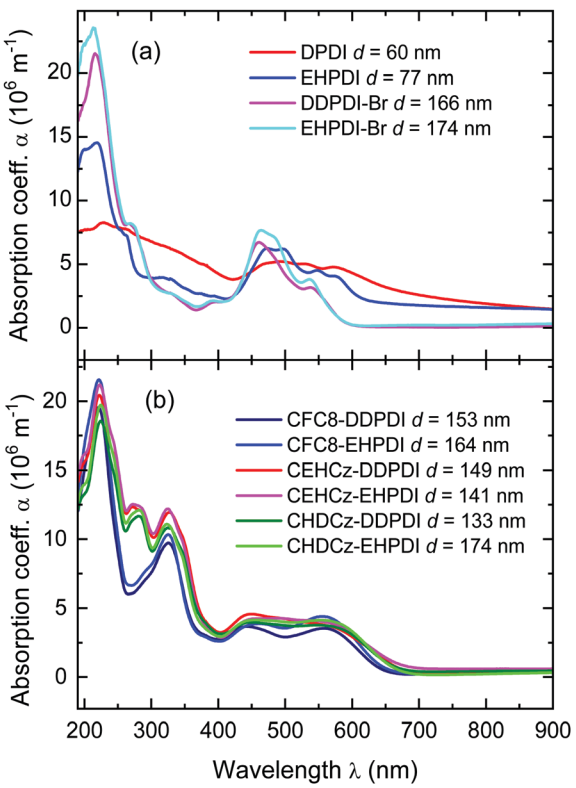

Fig. 5 UV-vis absorption spectra of (a) the **DDPDI** and **EHPDI** units, **DDPDI-Br** and **EHPDI-Br** monomers, and (b) the copolymers under study measured in thin films.

Table 4 Photophysical properties of the polymers measured in thin films (λ_{absmax} absorption maximum, λ_{PLmax} emission maximum, d film thickness). The main maxima are printed in bold

Copolymer	d (nm)	λ_{absmax} (nm)	λ_{PLmax}[a] (nm)
DDPDI	60	**228**, 492, 527, 570	660
EHPDI	77	**219**, **472**–496, 548s, 572s	634
DDPDI-Br	174	**217**, 267, 328, 394, **461**, 537	626
EHPDI-Br	166	**213**, 268, 328, 394, **461**, 536	616
CFC8-DDPDI	153	**221**, 325, **443**, 558	687
CFC8-DDPDI	141	**221**, 325, **445**, 561	687
CFC8-DDPDI	42	**223**, 330, 448, **566**	691
CFC8-EHPDI	164	**221**, 325, 462, **556**	718
CFC8-EHPDI	138	**221**, 325, 462, **558**	718
CFC8-EHPDI	35	**223**, 328, 463, **565**	709
CEHCz-DDPDI	149	**221**, 271, 327, **447**–553	700
CEHCz-DDPDI	130	**223**, 271, 329, **445**–544	699
CEHCz-DDPDI	35	**223**, 275, 333, **450**–560	702
CEHCz-EHPDI	141	**223**, 273, 325, 459–544	713
CEHCz-EHPDI	127	**223**, 271, 325, 454–542	713
CEHCz-EHPDI	49	**222**, 274, 327, 459–**561**	705
CHDCz-DDPDI	140	**225**, 281, 326, **450**, 556	704
CHDCz-DDPDI	133	**224**, 280, 327, **447**, 558	704
CHDCz-DDPDI	41	**225**, 281, 327, 460, **565**	704
CHDCz-EHPDI	174	**224**, 282, 324, **455**, 553	708
CHDCz-EHPDI	117	**224**, 280, 324, **448**, 567	708
CHDCz-EHPDI	42	**225**, 284, 324, 459, **570**	710

[a] Excitation wavelength at 554 nm.

The PL spectra of the model PDI units (**EHPDI**, **DDPDI**), PDI monomers (**EHPDI-Br**, **DDPDI-Br**) and copolymers measured in dilute chloroform solutions are displayed in Fig. 6. The emission spectra of all copolymers were broadband and structureless compared to the well-resolved PL spectra of **DDPDI**, **EHPDI**, **DDPDI-Br**, and **EHPDI-Br**, as shown for comparison. The **DDPDI** and **EHPDI** spectra showed a vibronic structure with maxima at 534 and 535 nm, respectively, and small Stokes shifts. Similarly, as in absorption, the broadening of the spectral bands due to the Franck–Condon progression in vibration modes was observed in the spectra of the **DDPDI-Br** and **EHPDI-Br** monomers, and a 12 nm redshift of the main maxima, which are located at 546 and 547 nm for **DDPDI-Br** and **EHPDI-Br**, respectively, was observed compared with **DDPDI** and **EHPDI**. The PL emission spectra of the copolymers are broadband with redshifted maxima and large Stokes shifts of more than 100 nm corresponding to excimer or aggregate emission.[22,55–57]

The spectra of the **CFC8-DDPDI** and **CFC8-EHPDI** copolymers with fluorene D units showed maxima at 661 and 660 nm, respectively (Table 3). The PL maxima of the copolymers with the carbazole D units were redshifted, located at 698 and 696 nm for **CEHCz-DDPDI** and **CEHCz-EHPDI**, respectively, and at 680 and 679 nm for **CHDCz-DDPDI** and **CHDCz-EHPDI**, respectively. The shapes of the excitation spectra of **DDPDI**, **EHPDI** and **DDPDI-Br**, **EHPDI-Br** were coincident with their absorption spectra. The excitation spectra of the copolymers were better resolved than their absorption spectra but roughly follow their shapes. The **DDPDI**, **EHPDI**, **DDPDI-Br**, and **EHPDI-Br** exhibited high PL quantum yield, η_{PL}, which significantly decreased in D–A copolymers (by a factor of *ca.* 5–50), which is in agreement with the excimer emission assignment. The **CFC8-DDPDI** copolymer exhibited

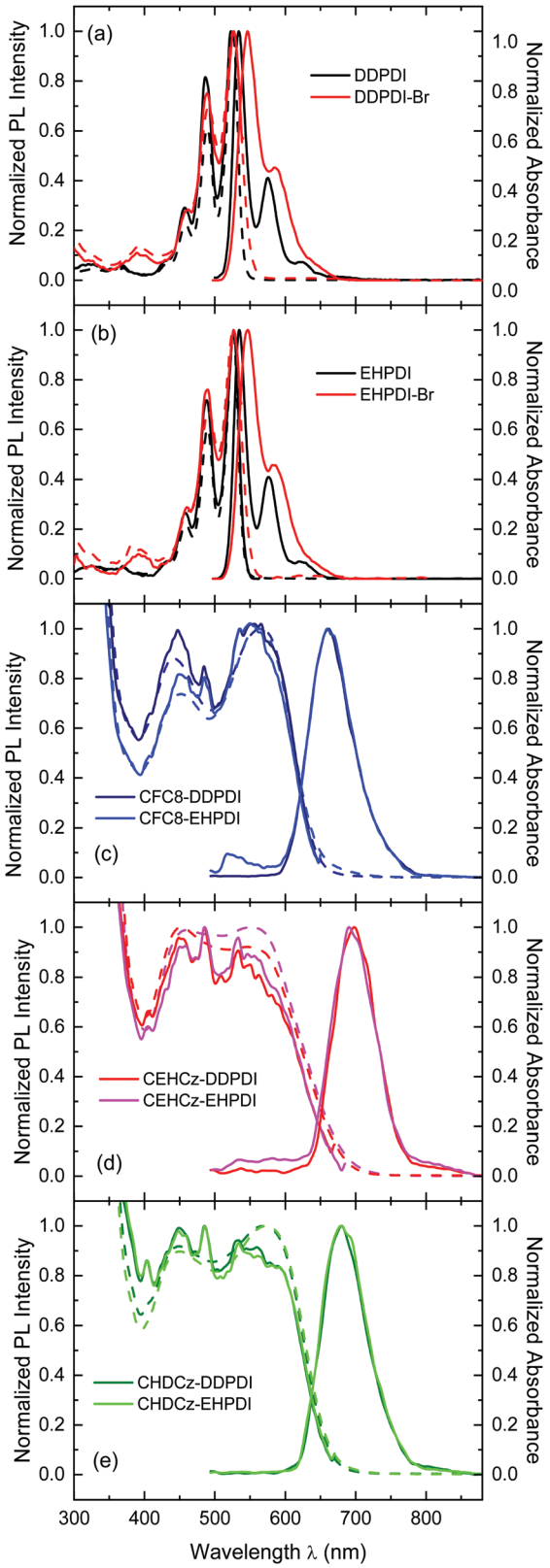

Fig. 6 PL excitation and emission spectra of (a) the **DDPDI** and **EHPDI** units, (b) the **DDPDI-Br** and **EHPDI-Br** monomers, and (c–e) the copolymers under study measured in dilute chloroform solutions.

the highest η_{PL} value of 0.2 of all copolymers under study, which is higher than the value of 0.15 seen for the **CFC8-EHPDI** with the same fluorene D unit but with 2-ethylhexyls on PDI instead of dodecyls.

The **CFC8-DDPDI** and **CFC8-EHPDI** copolymers with fluorene D units show higher η_{PL} than the copolymers with the carbazole D units. The η_{PL} is influenced by the side chain nature on the carbazole unit and on the PDI unit. Slightly higher η_{PL} values were determined for **CHDCz-DDPDI** and **CHDCz-EHPDI** with longer and bulkier heptadecan-9-yl side chains on carbazole than those for **CEHCz-DDPDI** and **CEHCz-EHPDI** with 2-ethylhexyl on the carbazole unit. The copolymers **CHDCz-EHPDI** and **CEHCz-EHPDI** with 2-ethylhexyls on the PDI unit showed slightly higher η_{PL} values than those of **CHDCz-DDPDI** and **CEHCz-DDPDI** with dodecyls on PDI, which is opposite the influence of PDI sidechains for copolymers with fluorene D unit. This indicates that the PDI sidechain influence is sensitive to the D–A strength in the backbone.

The PL spectra of the thin films are displayed in Fig. 7, and the characteristic data are summarized in Table 4. The PL spectra of **DDPDI**, **EHPDI**, **DDPDI-Br**, and **EHPDI-Br** thin films differ significantly when compared with their spectra in solutions due to the intermolecular interactions (aggregation), as was already observed and mentioned in the absorption spectra. Their emission spectra were broad, structureless and significantly redshifted compared with the solution spectra, indicating excimer and/or aggregate formation. The redshifts were more pronounced for the dodecyl-substituted PDI units than for the 2-ethylhexyl substitution. The same was observed for the monomers, for which the redshift was not very high, indicating that the substitution in bay positions can partially hinder the aggregation in films. The PL emission spectra of the copolymer films were broadband and structureless, similar to the solution spectra, but their maxima were redshifted compared to those in dilute solutions due to the enhanced planarity and intermolecular interactions. The PL maxima were located at 687 nm for **CFC8-DDPDI**, at 718 nm for **CFC8-EHPDI**, at 700 nm for **CEHCz-DDPDI**, at 713 nm for **CEHCz-EHPDI**, at 704 nm for **CEHCz-DDPDI** and at 708 nm for **CEHCz-EHPDI**. The differences in the PL emission maxima for the copolymer thin films were not as pronounced as in the solution spectra. The largest PL maximum redshift was observed for the **CFC8-EHPDI** thin films. The PL maxima of the copolymers with the 2-ethylhexyls on the PDI unit showed larger redshifts than the copolymers with dodecyl-substituted PDI; hence, their maxima were located at longer wavelengths than for the copolymers with the dodecyls. The excitation spectra were better resolved than the absorption spectra, but they roughly follow the absorption spectra shapes for all copolymers and monomers.

The relative PL efficiency of a thin film, Φ_{PLrel}, was evaluated and used to compare the PL efficiencies of the copolymers. The normalized Φ_{PLrel} values for the copolymers under study are shown in Fig. 8, where the normalized η_{PL} values of their solutions are displayed for comparison. The highest Φ_{PLrel} value was determined for **CFC8-DDPDI** thin films, similar to its solution. For the other copolymers, there was a significant difference in the efficiency dependence on the substitution

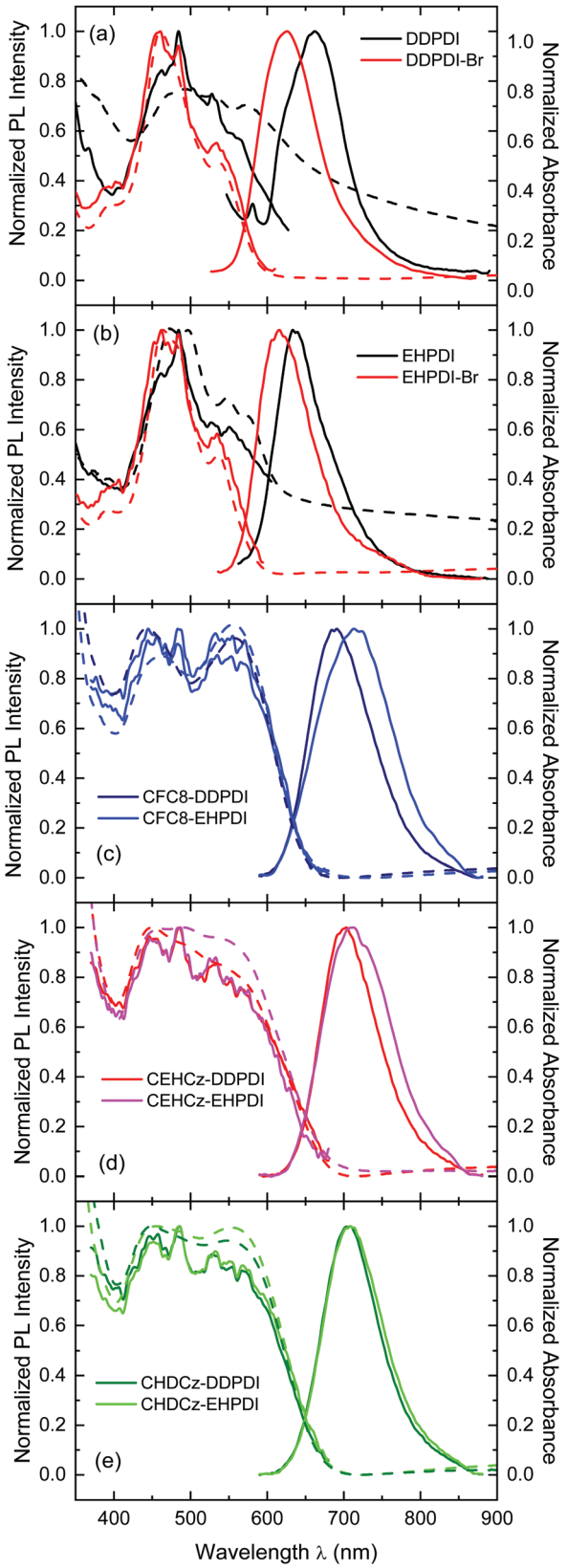

Fig. 7 PL excitation and emission spectra of (a) the **DDPDI** and **EHPDI** units, (b) the **DDPDI-Br** and **EHPDI-Br** monomers, and (c–e) the copolymers under study measured in thin films.

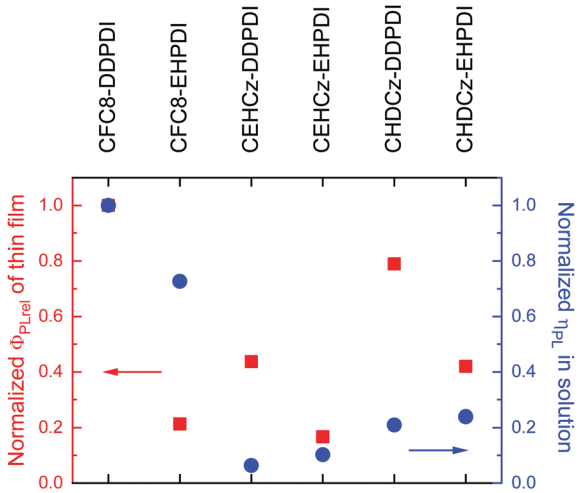

Fig. 8 Normalized relative efficiency, Φ_{PLrel}, of thin films (■) and normalized PL quantum yield, η_{PL}, in solution (●) for the copolymers under study.

in solution and thin films. The Φ_{PLrel} values of thin films are significantly higher for the copolymers with dodecyl substituted PDI units than for the copolymers with 2-ethylhexyls on the PDI unit, whereas the differences in the η_{PL} values of corresponding solutions were not as pronounced. The PDI alkyl substitution influenced not only the position of the PL maxima but also the PL efficiency.

Electrochemical properties

Cyclic voltammetry (CV) measurements were performed to obtain information on the electronic structure of the synthesized polymers. An example of representative CV curves of thin films coated on a Pt wire is displayed in Fig. 9. All copolymers exhibited two wave one-electron quasi-reversible reductions, whereas the oxidation was less reversible. Two pairs of peaks occurring at different potentials indicated the presence of two redox reactions. Upon the first reduction (at *ca.* −1 V *vs.* Ag/Ag^+), a carbonyl group on the PDI unit gains an electron to form PDI^-; to achieve charge neutrality, a cation dopes the negatively charged PDI unit. As the voltage decreased further, a second reduction occurred at the PDI unit (at *ca.* −1.2 V *vs.* Ag/Ag^+), resulting in another carbonyl group's reduction to PDI^{2-}. The peak current of the first reduction peak was notably less than that of the second reduction peak. When the potential was reversed, oxidation and the first de-doping of the PDI unit occurred (at *ca.* −1.05 V *vs.* Ag/Ag^+) as a higher peak than the second oxidation peak that occurred at the PDI unit upon increasing the potential further (at *ca.* −0.85 V *vs.* Ag/Ag^+). The peak separation ΔE_p of *ca.* 200 mV at a rate of 50 mV s^{-1} decreased with lower scan rates. ΔE_p was <200 mV for both reactions, and overlapping cyclic voltammogram curves at a fixed scan rate indicated that the redox reactions are reversible. The ionization potential (HOMO level), E_{IP}, and electron affinity (LUMO level), E_A, were estimated from the onset potentials, E_{onset}, of the oxidation and reduction peaks based on the reference energy level of ferrocene (4.8 eV below the vacuum level) using the equation E_{IP} (E_A) = $|-(E_{onset} - E_{ferr}) - 4.8|$ eV,

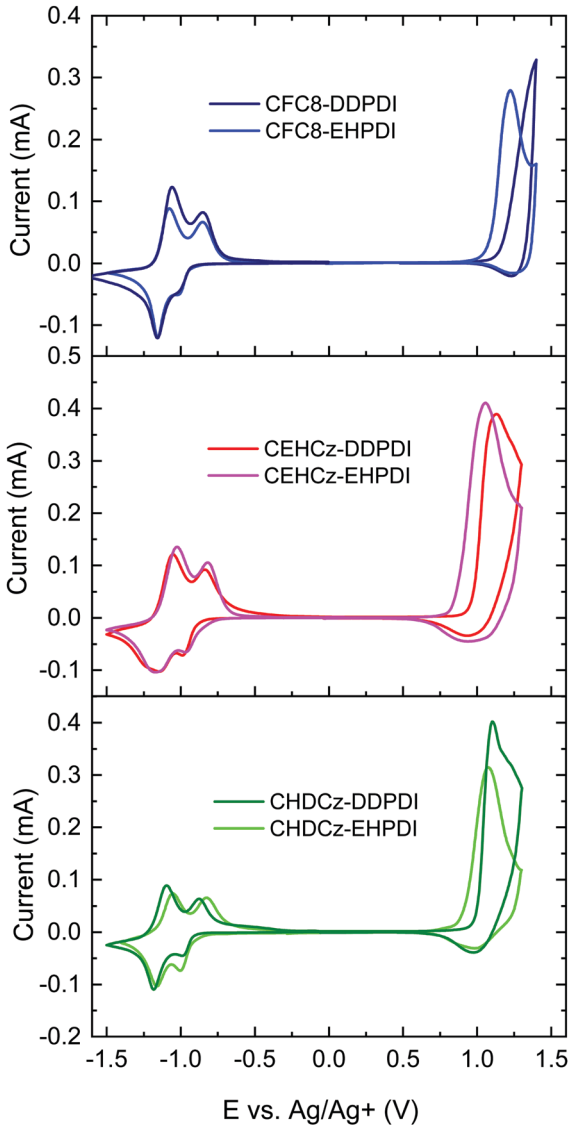

Fig. 9 Representative cyclic voltammograms of copolymer thin films coated on a Pt wire recorded at a scan rate of 50 mV s^{-1}.

where E_{ferr} is the half-wave potential for ferrocene *vs.* the Ag/Ag^+ electrode. The E_{IP} and E_A values were evaluated as averages from CV curves measured at a scan rate of 50 mV s^{-1} and are given in Table 5.

The ionization potential (5.63–5.9 eV) and electron affinity (3.82–3.91 eV) values were evaluated. The copolymers **CFC8-DDPDI**

Table 5 Electronic properties of the copolymers (E_{IP}: ionization potential; E_A: electron affinity; E_g^{elc}: electrochemical bandgap; E_g^{opt}: optical bandgap)

Copolymer	E_{IP} (eV) ($-E_{HOMO}$)	E_A (eV) ($-E_{LUMO}$)	E_g^{elc} (eV)	$E_g^{opt\text{-}d}$ (eV)	$E_g^{opt\text{-}i}$ (eV)
CFC8-DDPDI	5.91	3.86	2.05	1.98	1.83
CFC8-EHPDI	5.82	3.83	1.99	1.97	1.81
CEHCz-DDPDI	5.73	3.86	1.87	1.92	1.76
CEHCz-EHPDI	5.63	3.91	1.72	1.92	1.72
CHDCz-DDPDI	5.75	3.83	1.92	1.93	1.76
CHDCz-EHPDI	5.69	3.82	1.87	1.93	1.76

and **CFC8-EHPDI** with fluorene D units exhibited higher E_{IP} values than the copolymers with carbazole D units, which is in agreement with the stronger electron-donating capability of carbazole than that of fluorene D unit. The copolymers **CFC8-DDPDI**, **CEHCz-DDPDI**, and **CHDCz-DDPDI**, with dodecyls on the PDI unit, exhibited higher E_{IP} than those for the copolymers **CFC8-EHPDI**, **CEHCz-EHPDI**, and **CHDCz-EHPDI** containing branched 2-ethylhexyls on the PDI unit. Slightly higher E_A values were determined for **CEHCz-EHPDI** and **CHDCz-EHPDI** with branched 2-ehtylhexyls than those for the copolymers **CEHCz-DDPDI** and **CHDCz-DDPDI** with dodecyls.

The electrochemical bandgap values, E_g^{elc}, of approximately 2 eV were evaluated for the copolymers **CFC8-DDPDI** and **CFC8-EHPDI** containing fluorene D units and were slightly higher but still in good agreement with the optical bandgap values, $E_g^{opt\text{-}d}$, of 1.97–1.98 eV determined for direct allowed transition from thin film absorption spectra. The optical bandgap values for direct ($E_g^{opt\text{-}d}$) and indirect ($E_g^{opt\text{-}i}$) transitions were determined from the dependence of the absorption coefficient α on energy according to the relation $\alpha = \alpha_0(h\nu - E_g)^p$, where $h\nu$ is photon energy, E_g is the energy bandgap, and p is a constant depending on the type of electronic transitions, where p is 1/2 for direct and 2 for indirect transitions (*i.e.*, from the extrapolation of the linear dependence of α or $\alpha^{1/2}$ *vs.* E to α = 0 for direct and indirect transitions, respectively). The E_g^{elc} values of 1.72–1.92 eV were obtained for the copolymers with carbazole D units, which were lower than the corresponding $E_g^{opt\text{-}d}$ values and closer to the $E_g^{opt\text{-}i}$ values. The lowest E_g^{elc} value of 1.72 eV was evaluated for **CEHCz-EHPDI**. Our electrochemical values for **CFC8-EHPDI** and **CHDCz-EHPDI** correlate better with the optical bandgap than the only results available in the literature reported for the corresponding polymers. The electrochemical data available in the literature are E_{IP} = 5.93 eV and E_A = 3.61 eV, presenting an E_g^{elc} of 2.32 eV for the **CFC8-EHPDI** polymer (M_n = 13 600 and $Đ$ = 1.75), and E_{IP} = 5.83 eV and E_A = 3.66 eV, presenting an E_g^{elc} of 2.21 eV for **CHDCz-EHPDI** (M_n = 12 100 and $Đ$ = 1.62).[17] E_{IP} = 5.83 eV and E_A = 3.94 eV, presenting an E_g^{elc} of 1.89 eV for poly[*N*,*N*′-didodecylperylene-3,4,9,10-tetra-carboxydiimide-1,7-diyl-*alt*-9,9-dihexylfluorene-2,7-diyl] (M_w = 34 941 and $Đ$ = 1.55), and E_{IP} = 5.65 eV and E_A = 3.93 eV, presenting an E_g^{elc} of 1.72 eV for **CEHCz-DDPDI** (M_w = 35 787 and $Đ$ = 1.71).[36]

All of the copolymers showed interesting redox behaviour; therefore, we studied the spectral changes during oxidation (p-doping) and reduction (n-doping) by means of absorption spectroscopy, which enabled us to monitor the formation of ionic states (polarons and bipolarons). The evolution of the changes in the optical absorption spectra during oxidation and reduction were measured in thin films spin-coated onto indium-tin oxide (ITO) substrates and are displayed in Fig. 10 and 11. Absorption changes during oxidation were irreversible, whereas good reversibility was observed during the reduction. All of the copolymers under study exhibited qualitatively similar changes during the reduction cycle, but more pronounced differences between the copolymers with the fluorene and carbazole D units and a slight effect of nature of the alkyl chain attached to a PDI unit was observed during the oxidation. During oxidation,

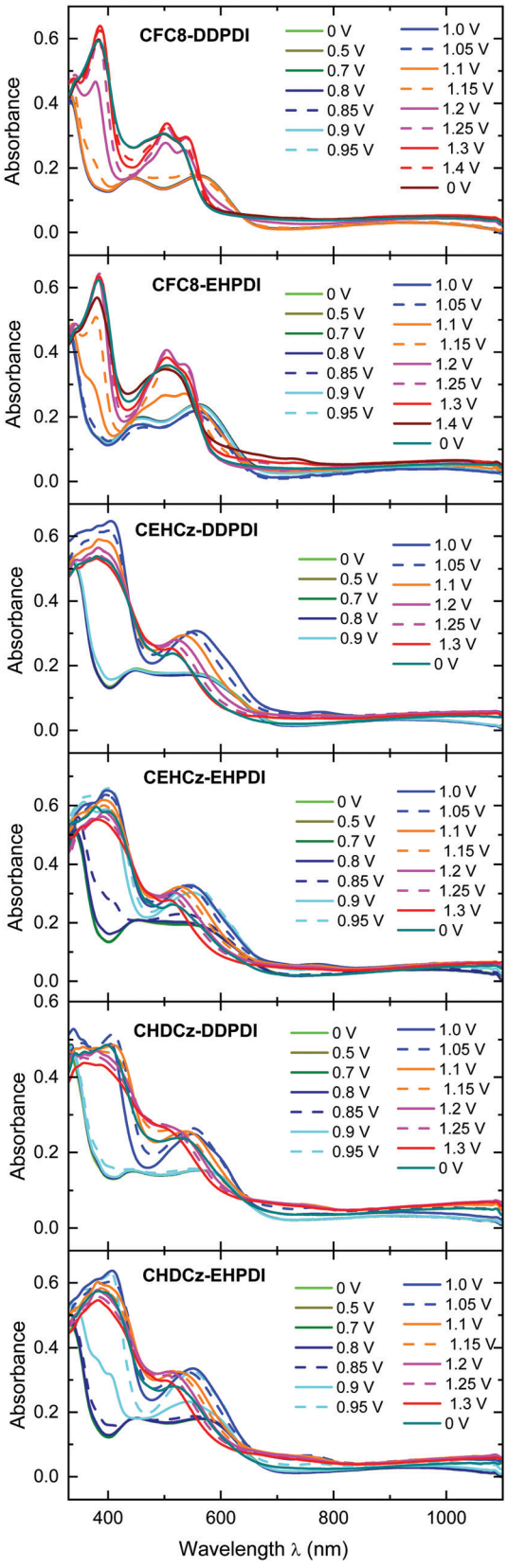

Fig. 10 Absorption spectra of the copolymers under study in thin films on ITO measured during the oxidation cycle *in situ* while changing the voltage in the range from 0 V (neutral state) to 1.3 V *vs.* Ag/Ag^+ in a stepwise manner.

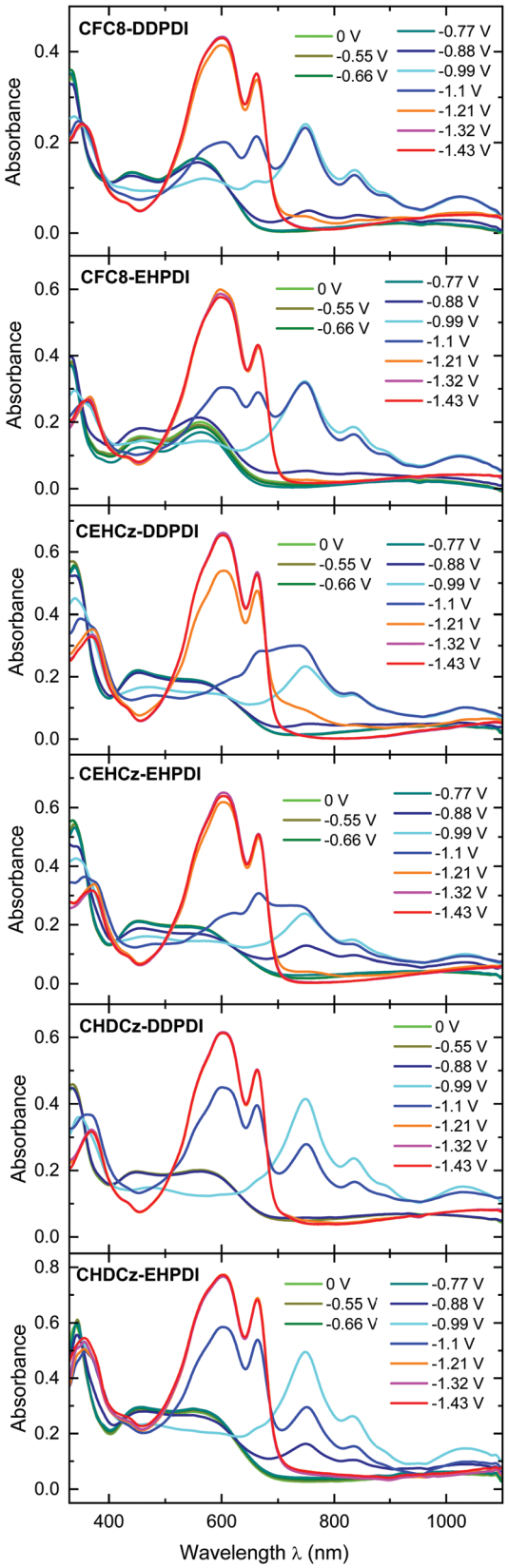

Fig. 11 Absorption spectra of the copolymers under study in thin films on ITO measured during the reduction cycle *in situ* while changing the voltage in the range from 0 V (neutral state) to −1.5 V *vs.* Ag/Ag^+ in a stepwise manner.

spectral changes started at approximately 1.15 and 1.1 V *vs.* Ag/Ag^+ for **CFC8-DDPDI** and **CFC8-EHPDI** with fluorene D units, respectively, when an increase in absorption at 350–400 nm and at 450–550 nm was observed. The changes in the maximum positions are summarized in Table 6. At 1.2–1.3 V *vs.* Ag/Ag^+, which is in the potential region exceeding the oxidation peak potential (see Fig. 9 and 10), new absorption bands with well resolved maxima at 378, 502 and 535 nm for **CFC8-DDPDI**, and 382, 504 and 534 nm for **CFC8-EHPDI** clearly appeared, and the absorption edge blueshifted when compared with the neutral state absorption spectra. In the copolymers with carbazole D units, the absorption changes during oxidation started at slightly lower potentials at approximately 0.9 and 0.95 V *vs.* Ag/Ag^+ for **CEHCz-DDPDI** and **CHDCz-DDPDI**, respectively, (copolymers with dodecyl-substituted PDI) and at 0.8 and 0.85 V *vs.* Ag/Ag^+ for **CEHCz-EHPDI** and **CHDCz-EHPDI**, respectively, (copolymers with 2-ethylhexyl-substituted PDI). At 1 V *vs.* Ag/Ag^+, broad bands with maxima at 405 and 556 nm for **CEHCz-DDPDI**, at 398 and 544 nm for **CEHCz-EHPDI**, at 404 and 550 nm for **CHDCz-DDPDI**, and at 407 and 550 nm for **CHDCz-EHPDI** were observed. With increasing potentials, blueshifts of the absorption maxima and absorption edge were detected. The band at approximately 550 nm was not resolved, as in the case of copolymers with fluorene D units. Only a slight effect of the nature of the alkyl chain attached to the PDI unit could be observed.

During the reduction, formation of anions and dianions with strong absorption in the visible region and NIR was observed (see Fig. 11). The spectral changes in absorption spectra started at approximately −0.8 V *vs.* Ag/Ag^+ with increasing absorption at long wavelengths. When the potentials reached the value exceeding the first peak potential (at −1 V *vs.* Ag/Ag^+), a new, strong absorption band with a clear maximum at approximately 750 nm appeared, and the formation of additional bands with maxima at 831–836 nm and at 1024–1033 nm in NIR was evident. This corresponded to anion formation. As the potential further decreased, the NIR absorbance decreased, and new absorption bands in the spectral region of 480–700 nm appeared. When the potential reached a second potential peak (at −1.3 V *vs.* Ag/Ag^+), the absorption maximum at 750 nm and the NIR absorption diminished, and two clear maxima at 598–603 nm and 662–665 nm corresponding to the dianion formed (Table 7). The dianion is not stable and reacts in air with oxygen to restore the parent neutral state, which can be reduced again electrochemically in an inert atmosphere to give the dianion. Such behaviour indicates that the copolymers could be promising for a biomimetic organic dye-based catalytic system[58] and that such reversible charging renders the D–A copolymers useful for controlled electron storage and release, similar to PDIs in aqueous media.[59] The electrochemical and spectroelectrochemical results also show potential for sensing applications such as in sensors for toxic compounds, such as hydrazine vapours, or for molecular oxygen.[60,61] PL quenching was found in the reduced state, as demonstrated in the solution chemically reduced by the addition of trimethylamine and can be seen in Fig. 12; additionally, PL quenching in thin films after placing them in the vapours of selected organic amines was demonstrated. A detailed sensing

Table 6 Absorption changes of polymer thin films on ITO substrates during oxidation (λ_{absmax}: absorption maximum). The main maxima are printed in bold

Copolymer	λ_{absmax} (nm)@0 V *vs.* Ag/Ag^+	λ_{absmax} (nm)@1 V *vs.* Ag/Ag^+/*1.2 V *vs.* Ag/Ag^+	λ_{absmax} (nm)@1.3 V *vs.* Ag/Ag^+/*1.4 V *vs.* Ag/Ag^+
CFC8-DDPDI	333, 444, 561	*337, **378**, 502, 535	**386**, 504, 538/***383**, 500
CFC8-EHPDI	334, 460, 559	*341, **382**, 504, 534	**384**, 504/***380**, 500
CEHCz-DDPDI	337, 450	**405**, 556	**379**, 511
CEHCz-EHPDI	332, 453	**398**, 544	**381**, 509 sh
CHDCz-DDPDI	337, 445, 563	338, **404**, 550	**358**, 385, 508 sh
CHDCz-EHPDI	337, 451, 564	**407**, 550	**382**, 506 sh

Table 7 Absorption changes of polymer thin films on ITO substrates during reduction (λ_{absmax}: absorption maximum). The main maxima are printed in bold

Copolymer	λ_{absmax} (nm)@0 V *vs.* Ag/Ag^+	λ_{absmax} (nm)@−1 V *vs.* Ag/Ag^+	λ_{absmax} (nm)@−1.32 V *vs.* Ag/Ag^+
CFC8-DDPDI	332, 441, 557	338, 569, **749**, 836, 1027	353, **601**, 662
CFC8-EHPDI	334, 457, 562	339, 567, **747**, 834, 1024	364, **598**, 665
CEHCz-DDPDI	340, 451	340, 472, 552, **749**, 832, 1033	371, **603**, 663
CEHCz-EHPDI	339, 453	342, 467, 568, **747**, 831, 1031	371, **603**, 665
CHDCz-DDPDI	337, 449, 563	348, 474, **749**, 834, 1029	369, **603**, 663
CHDCz-EHPDI	341, 455, 549	350, 466, **749**, 832, 1032	356, **603**, 663

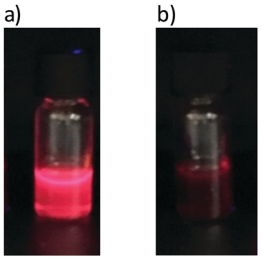

Fig. 12 Comparison of PL of **CFC8-DDPDI** in chloroform: (a) neutral and (b) reduced by trimethylamine addition.

study is beyond the scope of this paper and will be reported elsewhere.

Experimental

Materials and methods

All common chemicals were purchased from Sigma-Aldrich-Merck (Czech Republic) and used as received. Solvents were dried with Na/$LiAlH_4$ (THF), KOH (pyridine) or molecular sieves 4A (DMF) and distilled. The perylene-3,4,9,10-tetracarboxylic dianhydride (97%), sulfuric acid-d_2 (96–98 wt% in D_2O, 99.5 atom% D), trifluoroacetic acid-*d* (99.5 atom% D, CF_3COOD) calcined Celite® 577 fine filter aid, and 9,9-dioctylfluorene-2,7-diboronic acid bis(1,3-propanediol) ester (**FC8-B**) were purchased from Aldrich-Merck (CZ). 9-(Heptadecan-9-yl)-2,7-bis(4,4,5,5-tetramethyl-1,3,2-dioxaborolan-2-yl)carbazole (**HDCz-B**) was purchased from Ossila. 9-(2-Ethylhexyl)-2,7-bis(4,4,5,5-tetramethyl-1,3,2-dioxaborolan-2-yl)carbazole (**EHCz-B**) was synthesized according to literature.[62] The fuming sulfuric acid (oleum, 20 wt% of free SO_3) was purchased from Lach-ner (Neratovice, Czech republic). The catalyst tetrakis(triphenylphosphine)palladium(0) [99.99%, $Pd(PPh_3)_4$] was purchased from TCI. Silica gel 60 (0.063–0.200 mm, Merck) was used for column chromatography (columns ∅ 3 × 70 cm) of monomers and polymer purification. TLC was performed on Silicagel 60 F_{254} aluminium sheets (Merck), and the R_F values have the usual meaning (R_F = distance travelled by substance/distance travelled by solvent front). Aluminum oxide (neutral, Brockmann I, 50–200 μm) was purchased from Acros Organics.

^1H and ^{13}C NMR spectra were measured using an upgraded Bruker Avance DPX-300 spectrometer operating at 300.13 MHz and 75.45 MHz, respectively, or a Bruker Avance III 600 spectrometer operating at 600.27 MHz and 150.96 MHz, respectively. Hexamethyldisiloxane was used as an internal standard and $CDCl_3$ or sulfuric acid-d_2 as solvents. Fourier transform infrared (FTIR) spectra were measured using a PerkinElmer Paragon 1000 PC FTIR spectrometer *via* diamond attenuated total reflection (ATR). The size-exclusion chromatography (SEC) measurements were performed using a Pump Deltachrom (Watrex Comp.), autosampler Midas (Spark; with two columns of PL gel MIXED-C LS, particle size 5 μm), evaporative light scattering detector PL-ELS-1000 (Polymer Laboratories), and chloroform as a mobile phase. Polystyrene standards were used for the calibration and determination of weight-average (M_w), number-average (M_n) molecular weight and dispersity ($Đ = M_w/M_n$). Mass spectra were recorded using Bruker MICROTOFQ and Thermo LCQ-Deca ion trap mass instruments.

UV-vis spectra were measured on a PerkinElmer Lambda 35 UV/VIS spectrometer. Solvents of spectroscopic grade were used. The absorption spectra of thin films were also measured in the glove box using fiber optics connected to the spectrophotometer. Photoluminescence (PL) spectra were recorded using a PerkinElmer LS55 Fluorescence spectrophotometer. The PL quantum yield of the polymers in solution was calculated relative to the 4-dicyanomethylene-2-methyl-6-(4-(dimethylamino)styryl)-4*H*-pyran in DMSO, which was used as a standard (PL quantum yield 0.8)[63] for polymers and relative to the rhodamine 6G which was used as a standard (PL quantum yield 0.94)[64] for PDI units and monomers. Cyclic voltammetry (CV) was performed with a PA4 polarographic analyzer (Laboratory Instruments, Prague, CZ) with a three-electrode cell.

Platinum (Pt) wire electrodes were used as both working and counter electrodes. A non-aqueous Ag/Ag^+ electrode (Ag in 0.1 M $AgNO_3$ solution) was used as the reference electrode. CV measurements were made in an electrolyte solution of 0.1 M tetrabutylammonium hexafluorophosphate ($TBAPF_6$) in anhydrous acetonitrile under a nitrogen atmosphere in a glove box. Typical scan rates were 20, 50 and 100 mV s^{-1}. Spectroelectrochemical measurements were performed with a homemade cuvette, three electrode cell in a glove box connected to a Perkin PerkinElmer Lambda 35 UV/VIS spectrometer using fibre optics. The Pt wire and the non-aqueous Ag/Ag^+ electrode were used as the counter and the reference electrodes.

Thin films of copolymers were prepared by spin-coating from chloroform or 1,2-dichlorobenzene solutions onto fused silica substrates for the optical studies or ITO substrates for the spectroelectrochemical measurements, and coated onto a Pt wire electrode by dipping for CV measurements. All thin film preparations were conducted in a glove box under a N_2 atmosphere. All polymer films were dried in a vacuum (10^{-3} Pa) at 353 K for 2 h. The ITO glass substrates were purchased from Merck (Germany). Layer thicknesses (d) were measured using a KLA-Tencor P-10 profilometer.

Organic and polymer syntheses

Model PDI units EHPDI and DDPDI. *N*,*N*′-Bis(2-ethylhexyl)-perylene-3,4,9,10-tetracarboxydiimide (**EHPDI**) or *N*,*N*′-didodecyl perylene-3,4,9,10-tetracarboxydiimide (**DDPDI**) were synthesized according to published procedures.[65,66]

Bromination of perylene-3,4,9,10-tetracarboxylic dianhydride. The 7.85 g (20 mmol) of perylene-3,4,9,10-tetracarboxylic dianhydride (**I**) was weighted in a 250 mL three-neck round-bottom flask and 62.5 g (34 mL) of 96 wt% sulfuric acid (ρ = 1.83 g mL^{-1}) and 55.5 g (29 mL) of fuming sulfuric acid (ρ = 1.92 g mL^{-1}, oleum, 20% free SO_3) was added. The **I** was dissolved after oleum addition and mixing (6 h) and the solution was stirred overnight. The catalyst iodine (0.20 g, 0.78 mmol) was added, the reaction mixture was heated to 85 °C, and bromine (7.80 g, 48 mmol) was added dropwise over a time period of 8 h. After bromine addition, the reaction mixture was heated (85 °C) for an additional 14 h and then cooled to room temperature. The excess of bromine was removed by a gentle stream of argon, and water (50 mL) was added carefully. The resulting precipitate was separated by filtration (frit S3), washed with 70% (30 mL) and 40% (30 mL) sulfuric acid and a large amount of water, and dried in vacuum (oil pump, 2 days) to give a crude product as a red powder (yield: 11.69 g). The analysis of the product by 600 MHz ^{1}H NMR in deuterated sulfuric acid-d_2 (96–98 wt% in D_2O) revealed that 1,7- and 1,6-dibromo- and 1,6,7-tribromo-derivatives of **I** were formed in a ratio (wt%) of **II** : **III** : **IV** = 77 : 16 : 7 (Fig. S1, ESI†). Anal. calcd for $0.93(C_{24}H_6Br_2O_6)$ + $0.07(C_{24}H_5Br_3O_6)$ (555.63): 51.88% C, 1.08% H, 29.77% Br; found: 51.71% C, 1.07% H, 30.01% Br.

***N*,*N*′-Bis(2-ethylhexyl)-1,7-dibromoperylene-3,4,9,10-tetracarboxydiimide (EHPDI-Br) or *N*,*N*′-didodecyl-1,7-dibromoperylene-3,4,9,10-tetracarboxydiimide (DDPDI-Br).** In a 100 mL three-neck round bottom flask equipped with argon inlet, reflux condenser, septum and magnetic stirrer a suspension of brominated perylene-3,4,9,10-tetracarboxylic dianhydrides (**II** + **III** + **IV**, 2.0 g, *ca.* 3.56 mmol) in *N*-methyl-2-pyrrolidone (40 mL) and glacial acetic acid (10 mL) was heated to 60 °C for 25 min. Now, the 2-ethyl-1-hexylamine (1.18 g = 1.50 mL, 9.12 mmol) in the synthesis of **EHPDI-Br** or *n*-dodecylamine (1.69 g = 2.10 mL, 9.12 mmol) in the synthesis of **DDPDI-Br** was added slowly by a syringe *via* septum and the reaction mixture was heated under argon at 120 °C for 12 h and then cooled to room temperature. The content of reaction flask was poured into water (500 mL) and the precipitate was filtered off (frit S3), washed with methanol and dried to a constant weight. The crude **EHPDI-Br** (yield: 2.547 g) or **DDPDI-Br** (yield: 2.671 g) was collected and purified.

EHPDI-Br was purified by column chromatography on silica gel using dichloromethane/hexane (4 : 1 v/v) as eluent. Fractions containing **EHPDI-Br** (TLC in the same solvent, R_F = 0.47) were combined and characterized. Anal. calcd for $C_{40}H_{40}Br_2N_2O_4$ (772.56): 62.19% C, 5.22% H, 3.63% N, 20.69% Br; found: 62.25% C, 5.26% H, 3.61% N, 20.62% Br.

^{1}H NMR (600.27 MHz, $CDCl_3$, δ): 9.405 (d, 2H, J = 7.8 Hz, aromatic), 8.85 (s, 2H, aromatic), 8.626 (d, 2H, J = 7.8 Hz, aromatic), 4.17–4.08 (m, 4H, 2 × N–CH_2), 1.93 (m, 2H, 2 × >CH–), 1.40–1.23 (m, 16H, 8 × CH_2), 0.93 (t, 6H, J = 7.3 Hz, 2 × CH_3), 0.88 (t, 6H, J = 6.5 Hz, 2 × CH_3) (Fig. S2, ESI†). ^{13}C NMR (150.96 MHz, $CDCl_3$, δ): 163.3 (2 × C═O), 162.8 (2 × C═O), 138.1, 132.9, 132.8, 130.1, 129.2, 128.5, 127.0, 123.2, 122.8, 120.9 (20C aromatic), 44.5, 38.0, 30.8, 28.8, 24.1, 23.1, 14.2, 10.7 (16C aliphatic) (Fig. S4, ESI†).

DDPDI-Br was purified by column chromatography on silica gel using dichloromethane as eluent. Fractions containing **DDPDI-Br** (TLC in CH_2Cl_2/hexane = 3 : 1 v/v, R_F = 0.41) were combined and characterized. Anal. calcd for $C_{48}H_{56}Br_2N_2O_4$ (884.78): 65.16% C, 6.38% H, 3.17% N, 18.06% Br; found: 65.38% C, 6.58% H, 3.18% N, 17.95% Br.

^{1}H NMR (600.27 MHz, $CDCl_3$, δ): 9.378 (d, 2H, J = 8.4 Hz, aromatic), 8.81 (s, 2H, aromatic), 8.597 (d, 2H, J = 7.8 Hz, aromatic), 4.17 (t, 4H, J = 7.6 Hz, 2 × N–CH_2), 1.72 (m, 4H, 2 × N–C–CH_2), 1.42–1.26 (m, 36H, 18 × CH_2), 0.86 (t, 6H, J = 6.9 Hz, 2 × CH_3) (Fig. S3, ESI†). ^{13}C NMR (150.96 MHz, $CDCl_3$, δ): 162.8 (2 × C═O), 162.3 (2 × C═O), 138.0, 132.8, 132.7, 130.0, 129.1, 128.4, 126.9, 123.2, 122.7, 120.8 (20C aromatic), 40.9 (2C), 32.0 (2C), 29.7–29.4 (12C), 28.1 (2C), 27.2 (2C), 22.8 (2C), 14.2 (2C) (aliphatic) (Fig. S5, ESI†).

Synthesis of D–A copolymers poly[*N*,*N*′-dialkylperylene-3,4,9,10-tetracarboxydiimide-1,7-diyl-*alt*-9-alkylcarbazole-2,7-diyl or 9,9-dioctylfluorene-2,7-diyl]s. Donor-monomer (**FC8-B**, **EHCz-B**, or **HDCz-B**, 0.4338 mmol) was weighted into a dry preheated three-necked reactor equipped with a condenser, magnetic stirrer, septum, and argon inlet. The reactor was flushed with argon for 30 min. The acceptor-monomer (**EHPDI-Br** or **DDPDI-Br**, 0.4338 mmol) in degassed THF (30 mL) and degassed aqueous 2 M Na_2CO_3 (21 mL) was added by a syringe. The reaction vessel was purged with argon for 30 min to remove O_2. Finally, the catalyst $Pd(PPh_3)_4$ (21 mg, 2.0 mol % per both monomers) in degassed THF (5 mL) was added and the reaction mixture was refluxed (85 °C) under argon for 66 h. Then end-capping was

performed: (a) with phenylboronic acid pinacol ester (0.05 g, 0.25 mmol, 1 h reflux) and (b) with 2-ethylhexyl bromide (0.2 ml, 1.12 mmol, 2 h reflux). After cooling, the reaction mixture was separated into two layers. Water layer (aq. Na_2CO_3, bottom) was wasted and organic layer (crude polymer in THF, upper) was poured into an excess of methanol (700 mL). The precipitate was filtered off (S3), washed with water and methanol, and dried. The raw material was dissolved in chloroform, filtered through a short column of Celite® 577/aluminum oxide/silica gel 60 (*ca.* ∅ 4 × 3/3/3 cm) and the volume was reduced to *ca.* 15–20 mL by a rotary evaporator. The solution was precipitated into methanol (700 mL), the purified dark red polymer was filtered off (S3) and dried to a constant weight (yield: Y). The synthesized D–A polymers were characterized by SEC (M_w, M_n, $Đ$, P) in chloroform (Table 1) and by ^{1}H and ^{13}C NMR, and FTIR spectroscopy.

CFC8-DDPDI. Y = 0.3285 g (68%); ^{1}H NMR (300.13 MHz $CDCl_3$: CF_3COOD = 20 : 1 v/v, δ): 8.90–7.30 (m, 12H, aromatic H), 4.16 (br s, 4H, 2 × N–CH_2), 2.20–1.55 (br d, 8H, 2 × fluorene–CH_2 + 2 × N–C–CH_2), 1.50–0.45 (m, 72H, 30 × CH_2 + 4 × CH_3), (Fig. S6, ESI†). ^{13}C NMR (75.45 MHz, $CDCl_3$: CF_3COOD = 20 : 1 v/v, δ): 167.7 (2 × C═O), 167.0 (2 × C═O), 156.2, 145.1, 144.0, 138.7, 136.3, 133.4, 132.1, 130.5, 125.4, 124.4, 122.7, 118.9, 115.2, 111.4 (32C aromatic), 58.8 (═C(octyl)$_2$), 44.2, 42.8, 34.7, 32.4–32.1, 30.8, 29.8, 26.7, 25.4, 16.8 (40C aliphatic), (Fig. S7, ESI†). FTIR (ATR): 2922, 2852, 1698, 1660, 1588, 1460, 1431, 1402, 1326, 1245, 1162, 1125,1074, 1023, 860, 815, 760, 710, 625, cm^{-1} (Fig. S18, ESI†).

CFC8-EHPDI. Y = 0.2275 g (52%); ^{1}H NMR (300.13 MHz, $CDCl_3$, δ): 8.80–7.27 (m, 12H, aromatic H), 4.13 (br s, 4H, 2 × N–CH_2), 2.15–1.75 (br d, 6H, 2 × fluorene–CH_2 + 2 × ═CH–), 1.60–1.00 (m, 40H, 20 × CH_2), 0.88 (br s, 12H, 4 × CH_3), 0.75 (br s, 6H, 2 × CH_3) (Fig. S8, ESI†). ^{13}C NMR (75.45 MHz, $CDCl_3$, δ): 164.0 (2 × C═O), 163.5 (2 × C═O), 153.4, 142.7, 142.0, 141.7, 141.0, 135.2, 134.6, 132.8, 130.4, 129.6, 129.1, 128.0, 127.5, 123.6, 122.5, 122.3 (32C aromatic), 56.3 (═C(octyl)$_2$), 44.6, 40.4, 38.3, 31.9, 31.1, 30.8, 30.3, 30.1, 29.8, 29.4, 29.0, 24.4, 23.2, 22.7, 14.1, 10.8 (32C aliphatic) (Fig. S9, ESI†). FTIR (ATR): 2926, 2850, 1701, 1661, 1588, 1456, 1435, 1402, 1325, 1242, 1180, 1129, 1088, 1030, 862, 812, 753, 713, 629, cm^{-1} (Fig. S19, ESI†).

CEHCz-DDPDI. Y = 0.2530 g (58%); ^{1}H NMR (300.13 MHz, $CDCl_3$: CF_3COOD = 30 : 1 v/v, δ): 9.00–7.25 (m, 12H, aromatic H), 4.19 (br s, 6H, 3 × N–CH_2), 1.69 (br s, 5H, 1 × ═CH– + 2 × N–C–CH_2), 1.55–0.95 (m, 44H, 22 × CH_2), 0.90–0.40 (m, 12H, 4 × CH_3) (Fig. S10, ESI†). ^{13}C NMR (75.45 MHz, $CDCl_3$: CF_3COOD = 30 : 1 v/v, δ): 167.7 (2 × C═O), 167.3 (2 × C═O), 145.5, 142.6, 139.4, 138.9, 138.4, 136.4, 133.4, 132.1, 130.4, 129.8, 125.6, 124.4, 123.9, 122.7, 118.9, 115.1, 112.4, 111.4 (32C aromatic), 50.3 (Cz-N–C), 44.2, 42.4, 34.7, 33.7, 32.5–30.8, 29.8, 27.2, 25.6, 25.4, 16.8, 16.6, 13.4 (32C aliphatic) (Fig. S11, ESI†). FTIR (ATR): 2918, 2853, 1698, 1658, 1581, 1460, 1435, 1406, 1326, 1245, 1162, 1121, 1074, 1023, 998, 859, 808, 764, 746, 713, 625, cm^{-1} (Fig. S20, ESI†).

CEHCz-EHPDI. Y = 0.2510 g (65%); ^{1}H NMR (300.13 MHz, $CDCl_3$: CF_3COOD = 30 : 1 v/v, δ): 9.05–7.27 (m, 12H, aromatic H), 4.16 (br s, 6H, 3 × N–CH_2), 1.93 (br s, 3H, 3 × ═CH–), 1.65–1.00 (m, 24H, 12 × CH_2), 1.00–0.40 (m, 18H, 6 × CH_3) (Fig. S12, ESI†). ^{13}C NMR (75.45 MHz, $CDCl_3$: CF_3COOD = 30 : 1 v/v, δ): 167.7 (2 × C═O), 167.3 (2 × C═O), 146.4, 145.3, 142.5, 139.4, 138.6, 136.1, 133.3, 132.0, 130.3, 125.4, 124.4, 122.7, 119.0, 115.2, 112.4, 111.4 (32C aromatic), 47.6 (Cz-N–C), 42.3, 40.7, 33.4, 32.4, 31.3, 26.6, 25.7, 23.3, 16.7, 16.5, 13.2 (24C aliphatic) (Fig. S13, ESI†). FTIR (ATR): 2959, 2926, 2860, 1698, 1653, 1588, 1456, 1431, 1402, 1322, 1242, 1180, 1121, 1088, 1030, 998, 860, 808, 750, 713, 626, cm^{-1} (Fig. S21, ESI†).

CHDCz-DDPDI. Y = 0.3301 g (67%); ^{1}H NMR (300.13 MHz, $CDCl_3$: CF_3COOD = 20 : 1 v/v, δ): 9.10–7.25 (m, 12H, aromatic H), 4.55 (br s, 1H, Cz-N–CH═), 4.17 (br s, 4H, 2 × N–CH_2), 2.60–1.55 (m, 8H, Cz-N–C< $(CH_2)_2$ + 2 × N–C–CH_2), 1.50–0.90 (m, 60H, 30 × CH_2), 0.90–0.50 (m, 12H, 4 × CH_3) (Fig. S14, ESI†). ^{13}C NMR (75.45 MHz, $CDCl_3$: CF_3COOD = 20 : 1 v/v, δ): 167.6 (2 × C═O), 167.1 (2 × C═O), 146.6, 145.5, 142.6, 138.8, 136.4, 133.4, 132.1, 130.4, 125.2, 124.4, 124.0, 122.7, 118.9, 115.2, 111.4 (32C aromatic), 56.6 (Cz-N–C<), 44.2, 36.4, 34.6, 34.5, 32.3–32.1, 30.8–29.8, 25.4, 25.3, 16.8, 16.6 (40C aliphatic) (Fig. S15, ESI†). FTIR (ATR): 2918, 2853, 1698, 1654, 1585, 1453, 1431, 1400, 1326, 1245, 1162, 1125, 1074, 1023, 994, 860, 810, 738, 717, 640, cm^{-1} (Fig. S22, ESI†).

CHDCz-EHPDI. Y = 0.2990 g (68%); ^{1}H NMR (300.13 MHz, $CDCl_3$: CF_3COOD = 60 : 1 v/v, δ): 9.05–7.27 (m, 12H, aromatic H), 4.60 (br s, 1H, Cz-N–CH═), 4.14 (br s, 4H, 2 × N–CH_2), 2.25 (br s, 2H, 2 × ═CH–), 1.93 (br s, 4H, Cz-N–C< $(CH_2)_2$), 1.60–0.95 (m, 40H, 20 × CH_2), 0.88 (s, 12H, 4 × CH_3), 0.80–0.55 (br d, 6H, 2 × CH_3) (Fig. S16, ESI†). ^{13}C NMR (75.45 MHz, $CDCl_3$: CF_3COOD = 60 : 1 v/v, δ): 165.1 (2 × C═O), 164.5 (2 × C═O), 144.2, 142.7, 140.6, 140.1, 136.7, 136.0, 133.6, 130.6, 128.9, 127.8, 122.5, 121.9, 120.2, 116.4, 112.6, 108.8 (32C aromatic), 56.9 (Cz-N–C<), 45.0, 38.0, 33.8, 31.9, 30.8, 29.8, 29.5, 29.3, 28.7, 26.9, 24.0, 23.1, 22.7, 15.1, 14.1, 10.7 (32C aliphatic) (Fig. S17, ESI†). FTIR (ATR): 2951, 2925, 2857, 1698, 1654, 1588, 1456, 1431, 1402, 1322, 1242, 1180, 1125, 1088, 1030, 998, 863, 808, 742, 713, 640, cm^{-1} (Fig. S23, ESI†).

Conclusions

Six D–A copolymers containing *N*,*N*′-dialkylperylene-3,4,9,10-tetracarboxydiimide A units and three different D units [9,9-dioctylfluorene, 9-(2-ethylhexyl)carbazole or 9-(heptadecan-9-yl)carbazole], namely, poly[*N*,*N*′-dialkylperylene-3,4,9,10-tetracarboxydiimide-1,7-diyl-*alt*-9-alkylcarbazole-2,7-diyl or 9,9-dioctylfluorene-2,7-diyl]s, were synthesized by Suzuki coupling and characterized by elemental analysis, NMR, IR and SEC. They exhibited very good thermal stability in nitrogen and in air, indicating good oxidation stability, which is important for their applications. Contrary to the well-resolved absorption and PL spectra of the PDI unit in solutions, the absorption spectra and PL spectra of the copolymers, both in solutions and as thin films, consisted of broad bands in the visible spectral region corresponding to the π–π* transitions of the conjugated backbone. The PL maxima in thin films were redshifted when compared with those in the solution spectra, which corresponds to the backbone

planarity changes and excimer or aggregate formation. The relative PL efficiency, Φ_{PLrel}, values of the thin films were found to be significantly higher for the copolymers with dodecyl-substituted PDI units than for the copolymers with 2-ethylhexyls on the PDI unit, whereas the differences in the PL quantum yield, η_{PL}, values of the corresponding solutions were not as pronounced. The effects of the donor unit nature and side chains on electronic properties were revealed. More pronounced differences in ionization potential E_{IP} between the copolymers with the fluorene and carbazole D units were found; the copolymers with fluorene D units exhibited higher values than the copolymers with carbazole D units, corresponding to the stronger electron-donating capability of the carbazole unit. The copolymers **CFC8-DDPDI**, **CEHCz-DDPDI**, and **CHDCz-DDPDI**, with dodecyls on the PDI unit, exhibited higher E_{IP} than those for the copolymers **CFC8-EHPDI**, **CEHCz-EHPDI**, and **CHDCz-EHPDI** with branched 2-ethylhexyls on the PDI unit. All of the copolymers exhibited reversible reduction and irreversible oxidation. During reduction, formation of anions and dianions with strong absorption in the visible region and NIR was demonstrated. PL sensitivity to the reduction was also shown. New results concerning the influence of the alkyl side chains on the photophysical properties and also the spectroelectrochemical behaviour, which were gained, are important for photonic and electrochromic applications and for further development and optimization of polymeric materials.

Conflicts of interest

There are no conflicts to declare.

Acknowledgements

We would like to thank the Czech Science Foundation for supporting this work with grant 18-14683J.

Notes and references

1 X. W. Zhan, A. Facchetti, S. Barlow, T. J. Marks, M. A. Ratner, M. R. Wasielewski and S. R. Marder, *Adv. Mater.*, 2011, **23**, 268–284.
2 C. Tozlu, M. Kus, M. Can and M. Ersoz, *Thin Solid Films*, 2014, **569**, 22–27.
3 J. H. Jung, M. J. Yoon, J. W. Lim, Y. H. Lee, K. E. Lee, D. H. Kim and J. H. Oh, *Adv. Funct. Mater.*, 2017, **27**, 1604528.
4 W. Rekab, M. A. Stoeckel, M. El Gemayel, M. Gobbi, E. Orgiu and P. Samori, *ACS Appl. Mater. Interfaces*, 2016, **8**, 9829–9838.
5 H. Z. Chen, M. M. Ling, X. Mo, M. M. Shi, M. Wang and Z. Bao, *Chem. Mater.*, 2007, **19**, 816–824.
6 Z. Chen, Y. Zheng, H. Yan and A. Facchetti, *J. Am. Chem. Soc.*, 2009, **131**, 8–9.
7 R. Gvishi, R. Reisfeld and Z. Burshtein, *Chem. Phys. Lett.*, 1993, **213**, 338–344.
8 G. Griffini, L. Brambilla, M. Levi, M. Del Zoppo and S. Turri, *Sol. Energy Mater. Sol. Cells*, 2013, **111**, 41–48.
9 D. Pintossi, A. Colombo, M. Levi, C. Dragonetti, S. Turri and G. Griffini, *J. Mater. Chem. A*, 2017, **5**, 9067–9075.
10 G. D. Gutierrez, I. Coropceanu, M. G. Bawendi and T. M. Swager, *Adv. Mater.*, 2016, **28**, 497–501.
11 K. Y. Law, *Chem. Rev.*, 1993, **93**, 449–486.
12 W. E. Ford and P. V. Kamat, *J. Phys. Chem.*, 1987, **91**, 6373–6380.
13 H. C. Hesse, J. Weickert, C. Hundschell, X. L. Feng, K. Mullen, B. Nickel, A. J. Mozer and L. Schmidt-Mende, *Adv. Energy Mater.*, 2011, **1**, 861–869.
14 Y. Xiong, B. Wu, X. Zheng, Z. Zhao, P. Deng, M. Lin, B. Tang and B. S. Ong, *Adv. Sci.*, 2017, **4**, 1700110.
15 X. Zhan, Z. Tan, B. Domercq, Z. An, X. Zhang, S. Barlow, Y. Li, D. Zhu, B. Kippelen and S. R. Marder, *J. Am. Chem. Soc.*, 2007, **129**, 7246–7247.
16 H. Y. Wang, B. Peng and W. Wei, *Prog. Chem.*, 2008, **20**, 1751–1760.
17 E. Zhou, J. Cong, Q. Wei, K. Tajima, C. Yang and K. Hashimoto, *Angew. Chem., Int. Ed.*, 2011, **50**, 2799–2803.
18 E. Kozma and M. Catellani, *Dyes Pigm.*, 2013, **98**, 160–179.
19 J. Cann, S. Dayneko, J.-P. Sun, A. D. Hendsbee, I. G. Hill and G. C. Welch, *J. Mater. Chem. C*, 2017, **5**, 2074–2083.
20 A. Kalita, S. Hussain, A. H. Malik, N. V. V. Subbarao and P. K. Iyer, *J. Mater. Chem. C*, 2015, **3**, 10767–10774.
21 X. J. Liu, N. Zhang, J. Zhou, T. J. Chang, C. L. Fang and D. H. Shangguan, *Analyst*, 2013, **138**, 901–906.
22 Y. E, X. Ma, Y. Zhang, Y. Zhang, R. Duan, H. Ji, J. Li, Y. Che and J. Zhao, *Chem. Commun.*, 2014, **50**, 13596–13599.
23 N. Wu, C. Wang, B. R. Bunes, Y. Zhang, P. M. Slattum, X. Yang and L. Zang, *ACS Appl. Mater. Interfaces*, 2016, **8**, 12360–12368.
24 Y. Che, X. Yang, G. Liu, C. Yu, H. Ji, J. Zuo, J. Zhao and L. Zang, *J. Am. Chem. Soc.*, 2010, **132**, 5743–5750.
25 B. Roy, T. Noguchi, D. Yoshihara, Y. Tsuchiya, A. Dawn and S. Shinkai, *Org. Biomol. Chem.*, 2014, **12**, 561–565.
26 K. D. Belfield, M. V. Bondar, F. E. Hernandez and O. V. Przhonska, *J. Phys. Chem. C*, 2008, **112**, 5618–5622.
27 H. G. Wang, S. Yuan, D. L. Ma, X. L. Huang, F. L. Meng and X. B. Zhang, *Adv. Energy Mater.*, 2014, **4**, 1301651.
28 H. Banda, D. Damien, K. Nagarajan, A. Raj, M. Hariharan and M. M. Shaijumon, *Adv. Energy Mater.*, 2017, **7**, 1701316.
29 X. Zhu, X. Liu, W. Deng, L. Xiao, H. Yang and Y. Cao, *Mater. Lett.*, 2016, **175**, 191–194.
30 W. Deng, Y. Shen, J. Qian, Y. Cao and H. Yang, *ACS Appl. Mater. Interfaces*, 2015, **7**, 21095–21099.
31 B. A. Jones, A. Facchetti, M. R. Wasielewski and T. J. Marks, *J. Am. Chem. Soc.*, 2007, **129**, 15259–15278.
32 B. Russ, M. J. Robb, F. G. Brunetti, P. L. Miller, E. E. Perry, S. N. Patel, V. Ho, W. B. Chang, J. J. Urban, M. L. Chabinyc, C. J. Hawker and R. A. Segalman, *Adv. Mater.*, 2014, **26**, 3473–3477.
33 G. E. Park, H. J. Kim, S. Choi, D. H. Lee, M. A. Uddin, H. Y. Woo, M. J. Cho and D. H. Choi, *Chem. Commun.*, 2016, **52**, 8873–8876.
34 C. Li and H. Wonneberger, *Adv. Mater.*, 2012, **24**, 613–636.
35 J. Lee, R. Singh, D. H. Sin, H. G. Kim, K. C. Song and K. Cho, *Adv. Mater.*, 2016, **28**, 69–76.

36 E. F. Huo, Y. Zou, H. Q. Sun, J. L. Bai, Y. Huang, Z. Y. Lu, Y. Liu, Q. Jiang and S. L. Zhao, *Polym. Bull.*, 2011, **67**, 843–857.
37 M. Liu, J. Yang, C. Lang, Y. Zhang, E. Zhou, Z. Liu, F. Guo and L. Zhao, *Macromolecules*, 2017, **50**, 7559–7566.
38 S. Sharma, N. B. Kolhe, V. Gupta, V. Bharti, A. Sharma, R. Datt, S. Chand and S. K. Asha, *Macromolecules*, 2016, **49**, 8113–8125.
39 X. Jiang, Y. Xu, X. Wang, F. Yang, A. Zhang, C. Li, W. Ma and W. Li, *Polym. Chem.*, 2017, **8**, 3300–3306.
40 X. Meng, C. H. Y. Ho, S. Xiao, Y. Bai, T. Zhang, C. Hu, H. Lin, Y. Yang, S. K. So and S. Yang, *Nano Energy*, 2018, **52**, 300–306.
41 Z. Yin, J. Wei and Q. Zheng, *Adv. Sci.*, 2016, **3**, 1500362.
42 B. D. Naab, X. Gu, T. Kurosawa, J. W. F. To, A. Salleo and Z. Bao, *Adv. Electron. Mater.*, 2016, **2**, 1600004.
43 B. D. Naab, S. Zhang, K. Vandewal, A. Salleo, S. Barlow, S. R. Marder and Z. Bao, *Adv. Mater.*, 2014, **26**, 4268–4272.
44 B. A. Gregg, S.-G. Chen and R. A. Cormier, *Chem. Mater.*, 2004, **16**, 4586–4599.
45 Y. Che, A. Datar, X. Yang, T. Naddo, J. Zhao and L. Zang, *J. Am. Chem. Soc.*, 2007, **129**, 6354–6355.
46 W. Herbst and K. Hunger, *Industrial Organic Pigments*, Wiley-VCH, Weinheim, 3rd edn, 2004.
47 A. Böhm, H. Arms, G. Henning and P. Blaschka, Ger. Pat. Appl. 1997, vol. DE 19547209 A1, 1997, 127, 96569g.
48 F. Wurthner, V. Stepanenko, Z. J. Chen, C. R. Saha-Moller, N. Kocher and D. Stalke, *J. Org. Chem.*, 2004, **69**, 7933–7939.
49 P. Rajasingh, R. Cohen, E. Shirman, L. J. W. Shimon and B. Rybtchinski, *J. Org. Chem.*, 2007, **72**, 5973–5979.
50 C. Huang, S. Barlow and S. R. Marder, *J. Org. Chem.*, 2011, **76**, 2386–2407.
51 U. Rohr, C. Kohl, K. Mullen, A. van de Craats and J. Warman, *J. Mater. Chem.*, 2001, **11**, 1789–1799.
52 V. Cimrova, I. Kminek, D. Vyprachticky and V. Pokorna, *Polymer*, 2015, **59**, 298–304.
53 Y. J. Wang, Z. Y. Li, J. Q. Tong, X. Y. Shen, A. J. Qin, J. Z. Sun and B. Z. Tang, *J. Mater. Chem. C*, 2015, **3**, 3559–3568.
54 C. Shahar, S. Dutta, H. Weissman, L. J. W. Shimon, H. Ott and B. Rybtchinski, *Angew. Chem., Int. Ed.*, 2016, **55**, 179–182.
55 H. Liu, L. Shen, Z. Cao and X. Li, *Phys. Chem. Chem. Phys.*, 2014, **16**, 16399–16406.
56 J. M. McCrate and J. G. Ekerdt, *J. Phys. Chem. C*, 2014, **118**, 2104–2114.
57 K. E. Brown, W. A. Salamant, L. E. Shoer, R. M. Young and M. R. Wasielewski, *J. Phys. Chem. Lett.*, 2014, **5**, 2588–2593.
58 I. Ghosh, T. Ghosh, J. I. Bardagi and B. König, *Science*, 2014, **346**, 725–728.
59 E. Shirman, A. Ustinov, N. Ben-Shitrit, H. Weissman, M. A. Iron, R. Cohen and B. Rybtchinski, *J. Phys. Chem. B*, 2008, **112**, 8855–8858.
60 J. Wang, E. He, X. Liu, L. Yu, H. Wang, R. Zhang and H. Zhang, *Sens. Actuators, B*, 2017, **239**, 898–905.
61 I. S. Shin, T. Hirsch, B. Ehrl, D. H. Jang, O. S. Wolfbeis and J. I. Hong, *Anal. Chem.*, 2012, **84**, 9163–9168.
62 D. Vyprachticky, V. Pokorna, I. Kminek, V. Dzhabarov and V. Cimrova, *ECS Trans.*, 2014, **58**, 1–13.
63 M. Lesiecki, F. Asmar, J. M. Drake and D. M. Camaioni, *J. Lumin.*, 1984, **31–32**, 546–548.
64 A. M. Brouwer, *Pure Appl. Chem.*, 2011, **83**, 2213–2228.
65 Y. F. Wang, L. Zhang, G. J. Zhang, Y. Wu, S. Y. Wu, J. J. Yu and L. M. Wang, *Tetrahedron Lett.*, 2014, **55**, 3218–3222.
66 G. Boobalan, P. K. M. Imran, C. Manoharan and S. Nagarajan, *J. Colloid Interface Sci.*, 2013, **393**, 377–383.

